New BIOTECHNOLOGY 50 (2019) 52–59

Contents lists available at ScienceDirect

New BIOTECHNOLOGY

journal homepage: www.elsevier.com/locate/nbt

Full length Article

Glycerol metabolism of *Pichia pastoris* (*Komagataella spp.*) characterised by ^{13}C-based metabolic flux analysis

Màrius Tomàs-Gamisans[a], Anders Sebastian Rosenkrans Ødum[b], Mhairi Workman[d], Pau Ferrer[a,c], Joan Albiol[a,*]

[a] Department of Chemical, Biological and Environmental Engineering, Universitat Autònoma de Barcelona, Bellaterra, Cerdanyola del Vallès, Catalonia, Spain
[b] Department of Biotechnology and Biomedicine, Technical University of Denmark, Lyngby, Denmark
[c] Luxembourg Institute of Science and Technology, Luxembourg
[d] Novo Nordisk, Denmark

ARTICLE INFO

Keywords:
^{13}C-based metabolic flux analysis
Pichia pastorisKomagataella spp
Glycerol
Genome-Scale metabolic model

ABSTRACT

Metabolic flux analysis based on ^{13}C-derived constraints has proved to be a powerful method for quantitative physiological characterisation of one of the most extensively used microbial cell factory platforms, *Pichia pastoris* (syn. *Komagataella* spp.). Nonetheless, the reduced number of carbon atoms and the symmetry of the glycerol molecule has hampered the comprehensive determination of metabolic fluxes when used as the labelled C-source. Moreover, metabolic models typically used for ^{13}C-based flux balance analysis may be incomplete or misrepresent the actual metabolic network. To circumvent these limitations, we reduced the genome-scale metabolic model iMT1026-v3.0 into a core model and used it for the iterative fitting of metabolic fluxes to the measured mass isotope distribution of proteinogenic amino acids obtained after fractional ^{13}C labelling of cells with [1,3-^{13}C]-glycerol. This workflow allows reliable estimates to be obtained for *in vivo* fluxes in *P. pastoris* cells growing on glycerol as sole carbon source, as well as revising previous assumptions concerning its metabolic operation, such as alternative metabolic branches, calculation of energetic parameters and proposed specific cofactor utilisation.

Introduction

Glycerol is a side stream in conventional biodiesel production processes and its valorisation is therefore a highly interesting option in the development of a glycerol-based integrated biorefinery concept [1,2]. Glycerol is an attractive feedstock for production of high value added compounds using microbial fermentation processes [3–5]. Furthermore, the reduction degree of glycerol (4.67) is higher than that of glucose (4.0), and thus higher yields of certain metabolites can be obtained from it [6]. However, crude glycerol typically contains several impurities such as methanol [7], which is toxic for most microbes with the exception of methylotrophic microorganisms. *P. pastoris* is able to use glycerol and/or methanol efficiently as energy and carbon sources [8–10]. In fact, the conventional promoters used for heterologous gene expression in this yeast (namely, P_{GAP}, constitutive, and P_{AOX}, inducible) have been isolated from genes related to glycerol and methanol metabolism [11,12]. Indeed, *P. pastoris* has been shown to grow on media containing crude glycerol [13,14], and does not need to be genetically engineered for improved glycerol utilisation, as done in other species like *S. cerevisiae*, [15–17], due to a more efficient glycerol transport system [16]. These attributes make *P. pastoris* a cell factory of high potential for the development of glycerol biorefineries.

However, there are few systematic studies characterising growth of *P. pastoris* on glycerol as a sole carbon source [18,19]. Early ^{13}C-labelling experiments (CLE) performed with *P. pastoris* using glucose or glycerol as sole carbon sources were based on biosynthetically directed fractional (BDF) ^{13}C-labeling of proteinogenic amino acids with 2D-NMR, enabling the determination of metabolic flux ratios (METAFoR) [20]. This methodology relies on the identification of conserved C—C bounds in proteinogenic amino acids after feeding cells with a mixture

Abbreviations: BDF, Biosynthetically directed fractional 13C-labeling; CI, 95% confidence interval; DMFDMA, *N*-dimethyl-amino-methylene-methyl-esters; ECF, *N*-ethoxycarbonyl-amino ethyl-esters; ECT, Electron transport chain; GC–MS, Gas chromatography mass spectrometer; GRH, Growth rate hypothesis; GSMM, Genome-scale metabolic model; METAFoR, Metabolic flux ratio analysis; MFA, Metabolic flux analysis; MID, Mass isotopomer distribution; PPP, Pentose phosphate pathway; SEM, Standard error of the mean; TCA, Tricarboxylic acid cycle; τ, tau, residence time of the bioreactor (h)

* Corresponding author.
E-mail addresses: joan.albiol@uab.cat, joan.albiol@uab.es (J. Albiol).

https://doi.org/10.1016/j.nbt.2019.01.005
Received 28 March 2018; Received in revised form 11 January 2019; Accepted 13 January 2019
Available online 17 January 2019
1871-6784/ © 2019 Elsevier B.V. All rights reserved.

of unlabelled and ^{13}C-uniformly labelled glucose as substrate [21,22]. However, the information derived using this technique when using labelled substrates with a low number of carbons such as glycerol, limits its application [18,20]. In addition, ^{13}C-based metabolic flux studies reported so far typically rely on metabolic models based on pre-existing knowledge of the biochemical pathways of central carbon metabolism, including the amino acid biosynthesis pathways [18]. Such models have been used extensively to improve metabolic flux determination using the available experimental ^{13}C datasets [9,23–25], with only minor modifications based on direct experimental observations, such as that glyoxylate pathway or malic enzymes are not operative under the studied/similar growth conditions [8].

Building such models simply by combining well-known classical pathways may easily result in a derived model with missing steps or pathways relevant for the experimental conditions under study. As the ^{13}C based method for metabolic flux determination does not include cofactor balances (typically NAD(H)/NADP(H)), verification of those balances after the metabolic fluxes have been determined may reveal those inconsistencies in the underlying model. One way to overcome such inconvenience could be the use of a genome-scale metabolic model (GSMM).

A genome-scale description of *P. pastoris* metabolism has been developed through different versions such as the iMT1026 GSMM [26], which was subsequently adapted for growth on glycerol and methanol [19]. *A priori*, this GSMM would be an alternative of choice for ^{13}C-MFA, due to its inclusion of a more complete number of pathways. Nevertheless, large-scale ^{13}C-MFA has significant limitations such as the requirement for an accurate and complete atom transition mapping. Although there are databases including the reaction atom mapping of biological pathways, GSMM-specific reactions would require an additional effort to accurately annotate atom transitions. Another important hindrance for genome-scale ^{13}C-MFA is the resulting huge number of variables that significantly impact computational complexity and performance, as well as the difficulty or even impossibility in resolving all fluxes due to the robustness and redundancy of metabolic pathways, which include parallel and alternative pathways and cell compartmentalization [27]. Consequently, nowadays GSMMs are still not a practical alternative to core metabolic models. Indeed, it has been concluded [28] that reducing GSMMs down to a size similar to the currently used core metabolism models used in ^{13}C-MFA would be a feasible alternative to the use of full GSMMs. In this regard, several algorithms for reducing GSMMs to core models have been developed. One method that appears particularly suited to our purpose is NetworkReducer [29], which allows the information derived from previous ^{13}C studies to be taken into account, such as the network topology pathways shown to be active - in the experimental conditions tested. Briefly, this is achieved by protecting relevant reactions and applying phenotypic constraints while the algorithm successively eliminates or combines reactions until a minimal model that fulfils all those constraints is obtained. This method has been recently employed in *E. coli* to produce a new core model (EColiCore2) producing flux distributions equivalent to those generated by the original GSMM [30].

In this study, the genome-scale metabolic model iMT1026 v3.0 [19] is reduced to a glycerol-specific core model. This is further used for ^{13}C-MFA of *P. pastoris* growing on glycerol as carbon source at different growth rates. In order to circumvent the limitation of using a 3C-substrate, a 1- and 3-positionally labelled glycerol was used in place of a uniformly labelled substrate, together with the measurement of proteinogenic amino acid content and subsequent iterative fitting of metabolic fluxes to the measured mass isotope distributions (MIDs). Although this method does not allow the level of resolution achieved in non-stationary CLE, it is shown that such an approach enables improved accuracy of the resolved fluxes in comparison with previous metabolic flux profiling studies based on METAFoR analysis datasets.

Materials and methods

Strain and cultivation conditions

The *Pichia pastoris* X-33 strain (Invitrogen-Thermofisher, Carlsbad, CA, USA) was used throughout this study. Duplicate carbon-limited chemostat cultivations were performed using a Sartorius 0.5-L bioreactor (Sartorius AG, Göttingen, Germany) at dilution rates (D) of 0.05, 0.10 and 0.16 h^{-1} with a working volume of 0.3 L maintained by a gravimetrically controlled peristaltic pump. Chemostat cultivations were performed for at least 5 residence times (τ) prior to labelling.

Batch and chemostat media were adapted from [31] by reducing carbon and nitrogen source concentrations to yield an approximate final biomass of 6 g/L when the steady state was reached. Thus, in brief, batch medium contained: 9.98 g/L glycerol, 0.46 g/L citric acid, 3.15 g/L $(NH_4)_2HPO_4$, 0.006 g/L $CaCl_2{\cdot}2H_2O$, 0.225 g/L KCl, 0.125 g/L $MgSO_4{\cdot}7H_2O$, 0.5 mL Biotin (0.2 g/L), and 1.15 mL PTM1 trace salts stock solution (prepared as described in [31]). The pH value was adjusted to 5.0 with 25% HCl. Chemostat medium contained: 10 g/L glycerol, 0.818 g/L citric acid, 4.35 g/L $(NH_4)_2HPO_4$, 0.01 g/L $CaCl_2{\cdot}2H_2O$, 1.7 g/L KCl, 0.65 g/L $MgSO_4{\cdot}7H_2O$, 1.0 mL Biotin (0.2 g/L), 1.6 mL PTM1 trace salts stock solution and 0.2 mL/L of antifoam glanapon 2000 (Konc, Bussetti, Vienna, Austria).

An inoculum was cultivated overnight at 30 °C, 150 rpm in a 0.5-L shake flask containing 75 mL of basal medium with glycerol and supplemented with biotin (1% yeast nitrogen base, 4×10^{-5} % biotin, 1% glycerol). The bioreactor was inoculated at an initial OD_{600} of 0.3 – 0.5. Once glycerol was exhausted, continuous cultivations were started at the corresponding flow rate. The aeration rate was 1 vvm and the off-gas O_2 and CO_2 concentrations were measured using a Prima Pro Process Mass Spectrometer (Thermo Fisher Scientific). Temperature was maintained at 25 °C, the stirring rate was 500 rpm and a pH value of 5.0 was controlled by automatic addition of 15% ammonia.

Labelling experiment and biomass harvest

After a minimum of 5τ of continuous cultivations with non-labelled glycerol, the feed was switched to the labelled medium. Labeled feed medium composition was the same as the unlabeled, but replacing glycerol by 20% [1,3-^{13}C]-glycerol (CortecNet) and 80% unlabeled glycerol. Labeled medium was feed for at least 2τ. Culture samples (50–100 mL) were collected, centrifuged (15 min, 16,000 g), the supernatant discarded and pellets frozen in liquid N_2 and stored at −80 °C for further extraction and analysis of proteinogenic amino acids.

Biomass and exometabolite analysis

Cell density and dry cell weight

Cell density was monitored by optical density at 600 nm. Dry cell weight (DCW) was measured in duplicate gravimetrically. Briefly, a known volume of sample (5–10 mL) was filtered through dried preweighed 0.45 µm polyether sulfone filters (Frisenette, Knebel, Denmark) and washed with distilled water. Filters were dried in a microwave oven at 150 W for 20 min, cooled in a desiccator for at least 2 h and finally weighted.

Exometabolite analysis

Samples taken for external metabolite analysis were filtered through a 0.22 µm syringe filter and stored at −20 °C until subsequent analysis. Glycerol, was the only peak detected in HPLC analyses performed as described in [32].

Proteinogenic amino acid MID determination

Amino acid extraction, derivatization and GC–MS analysis

Mass Isotope distribution of the proteinogenic amino acid (MID)

was determined as described in [33]. Briefly, 5 mg of biomass pellets were hydrolyzed with 6 M hydrochloric acid at 105 °C for 16 h. Once at room temperature, samples were dried for 3 h under a stream of nitrogen. Samples were redissolved in water and filtered through Strata SCX (100 mg, 1 cc, Phenomenex, Torrance, CA, USA) columns and washed with 50% ethanol to remove impurities. Samples were eluted with 1 N NaOH and, in addition, with the elution solution [33]. Two types of derivatives were prepared for GC–MS analysis: *N*-ethoxycarbonyl-amino ethyl-esters (ECF) and *N*-dimethyl-amino-methylene-methyl-esters (DMFDMA) following the accurate protocol described in [33]. Derivatized amino acid samples were analyzed in a GC–MS Agilent 6890 gas chromatograph coupled to an Agilent 5973 quadruple MS according to the specified settings [33]. GC/MS Translator (Agilent) was used to convert the resulting row data files into those readable for Agilent Mass Hunter Qualitative Analysis software.

MID correction for natural isotopes and washout kinetics

MIDs are uncorrected for naturally labelled atoms other than carbon backbone [34,35]. OpenFlux [36] was used to correct the MID of each amino acid according to the expected fragmentation ions obtained in GC–MS analysis [37]. In addition, biomass was harvested at 2 τ after the onset of labelling and thus the fraction of labelled biomass ($X_{labelled}$) at the steady state was calculated according to a first-order wash-out kinetics [18]: $X_{labelled} = 1 - e^{-t/\tau}$, where t is the labelling time and τ the residence time of the chemostat. Corrected MIDs for each experimental replicate and corresponding analysed peaks from each corresponding derivatisation method can be found in Supplementary file S2, Table S2.

Statistical analysis

Chemostat cultivation data were checked for consistency using elemental mass balances and common reconciliation procedures [38]. The biomass molecular formula used was selected according to the specific biomass composition of *P. pastoris* growing on glycerol [19]. In all the cultivation sets, statistical consistency test was passed with a confidence level of 95%. Consequently, there was no evidence of gross measurement errors.

Core model generation

In order to obtain a representative network of the central carbon metabolism of *P. pastoris*, including all the relevant reactions, a core model (*PpaCore*) was derived from the iMT1026 v3.0 model using NetworkReducer [29] with CellNetAnalyser 2016.1 [39] under Matlab 2011. A detailed procedure and commands for model reduction can be found in Supplementary File S1. Default flux constraints for glycerol growth as the only possible carbon source were set. Since according to our previous work [19], there are important differences when comparing biomass compositions representing growth using different carbon sources, a specific biomass equation for glycerol was used in the present case. On the other hand, in the full genome-scale metabolic model used, there is only one biomass equation from an average biomass composition, as there are no statistically-significant differences when comparing the composition of different growth rates using this carbon source. Maximal growth rate in the reduced network was constrained to be 99.9% of the maximal growth rate for the iMT1026 v3.0 (here *PpaGS*, meaning '*P. pastoris* Genome-Scale') corresponding to the glycerol chemostat cultivations in our previous work [19]. In a first step, 46 reactions of central carbon metabolism were protected (Supplementary File S1) and *PpaGS* was reduced to a pruned model (*PpaPruned*). Subsequently, *PpaPruned* was further reduced to *PpaCore* by a compressing procedure with a new set of 56 protected reactions (Supplementary File S1). For numerical reasons, the 'cof' metabolite was removed from the biomass equation. The resulting *PpaCore* was tested for growth in glycerol and the same maximal growth rates obtained in *PpaGS* were achieved for a constrained uptake of glycerol.

^{13}C-Metabolic flux analysis (^{13}C-MFA)

Flux calculations were performed with OpenFLUX [36] under Matlab 2011 using FMINCON from Matlab's optimization toolbox. Before performing MFA, *PpaCore* was adapted to OpenFLUX requirements in three steps: (1) each reversible reaction was replaced by two paired irreversible reactions; (2) reactions mapping label distribution in the measured proteinogenic amino acids were added according to the appropriate compartmentalization [20]; (3) carbon atom transition equations were added according to previous *P. pastoris* models [9] and databases [40]. In order to avoid biased solutions, O_2, reduction equivalents, energetic cofactors and additional non-carbon-balanceable metabolites were defined as excluded metabolites. Moreover, those reactions in *PpaCore* that uniquely contained excluded metabolites were also removed from the final model for ^{13}C-metabolic flux calculations. The resulting model (Supplementary File S2, Table S1) was used for ^{13}C-MFA. Experimental MIDs showed an average deviation below 5% and the model was fitted to the experimental data by the least squares method detailed in [41] using the measured glycerol uptake rate and specific biomass generation rates as constraints. The parameter estimation procedure was repeated 100 times. Subsequently, the solution cluster with lower residual error was used for sensitivity analysis using the non-linear approach of [42]. Sensitivity analysis was performed in order to find the lower and upper confidence interval boundaries of calculated fluxes at a 95% confidence level [36]. Default configuration settings were used for the sensitivity analysis. In those cases where it was impossible to determine individually the forward and reverse fluxes, only the net fluxes were calculated and subjected to sensitivity analysis. Flux fitting to ^{13}C MID was performed individually for each experimental replicate and subsequently averaged. The main results were depicted using Omix graphic software [43].

Calculation of redox cofactor regeneration rates and energy requirements

Rates for redox cofactor regeneration and ATP synthesis were derived after calculation of the other fluxes. Once the solution of the metabolic system was determined, estimated fluxes were further used to calculate the remaining reaction fluxes that contained excluded metabolites. Redox cofactor balance was checked and any surplus of reduction equivalents (NADH both cytosolic and mitochondrial) was considered a source of electrons transferred to the electron transport chain (ECT). Thus, assuming complete electron transfer from the surplus reduction equivalents to ETC and taking into account the oxygen requirements for biomass synthesis (included in the full biomass equation), the oxygen uptake rate could be calculated and compared to the experimental values. In addition, since the model includes the complete ETC with proton translocation to the mitochondrial intermembrane space and the corresponding reaction for ATP synthesis [26], a theoretical maximal ATP generation rate could be estimated. The total ATP generation was taken into account later for calculating the energetic parameters. Essentially, two parameters were determined: growth and non-growth associated maintenance energy (GAME and NGAME, respectively) according to Pirt's equation [44] and applying a linear regression between ATP generation and growth rates [45]. The y-intercept would correspond to the NGAME ($\mu = 0.0\ h^{-1}$) and the slope to GAME (Supplementary Figure S1). Those values can be later compared to those obtained using the complete *PpaGS* model.

Results and discussion

Macroscopic growth parameter characterisation

Despite the increasing interest in using glycerol as feedstock for microbial biorefineries, there is limited information on the physiology of *P. pastoris* growing on such carbon source. In a recent study [19], we performed a series of cultivations at different growth rates using

Table 1
Reconciled macroscopic growth parameters for glycerol cultivations at different growth rates. D_{SP} (h^{-1}) corresponds to the set point dilution rate and D_{exp} (h^{-1}) to the experimentally measured D. q_S, q_{O2} and q_{CO2} are expressed in mmol · g_{DCW}^{-1} h^{-1}. Units for q_X are Cmmol · g_{DCW}^{-1} h^{-1}.Y_{XS} represents biomass yield (g_X $^{-1}$). RQ is the respiratory quotient.

D_{SP}	0.05	0.10	0.16
D_{exp}	0.046 ± 0.006	0.098 ± 0.009	0.166 ± 0.006
q_S	−0.72 ± 0.11	−1.45 ± 0.13	−2.52 ± 0.14
q_X	1.62 ± 0.21	3.43 ± 0.31	5.89 ± 0.23
q_{CO2}	0.55 ± 0.12	0.93 ± 0.07	1.65 ± 0.18
q_{O2}	−0.90 ± 0.18	−1.66 ± 0.14	−2.89 ± 0.25
Y_{XS}	0.70 ± 0.02	0.73 ± 0.01	0.72 ± 0.01
RQ	0.60 ± 0.02	0.56 ± 0.01	0.57 ± 0.01

glycerol as sole carbon source. These data allowed comprehensive analysis of the effects of growth rate on biomass composition.

Here, a new series of carbon-limited chemostat cultivations using glycerol as sole carbon source was performed at 3 different dilution rates (corresponding to a low, mid and high ranges) that had already been tested previously [19,20], namely 0.05, 0.10 and 0.16 h^{-1}. In order to obtain equivalent datasets, the culture medium composition was the same as in [19], except for glycerol concentration in the feed medium, which was reduced to obtain a lower steady state biomass concentration.

In agreement with [19], *P. pastoris* cells grown under these conditions showed no by-product secretion and residual glycerol in the broth samples was below the detection limit of the analytical method. All the measured external macroscopic fluxes showed a clear correlation with the growth rate ($R^2 > 0.99$), consistent with [19], where a linear range for the cell's macroscopic variables when growing on glycerol was established between 0.05 and 0.16 h^{-1} growth rate. Biomass yields (Y_{XS}) ranged between 0.70 – 0.72 g_X g_S^{-1} (Table 1). These values are in the upper range of Y_{XS} previously reported for glycerol as C-source [19] and are also in agreement with biomass yields on glycerol reported for other yeast species [46]. Similarly, the average experimental RQ (0.58 ± 0.02) was close to 0.63 ± 0.03, the average RQ experimentally determined previously for glycerol-grown cells. Hence, despite reducing the carbon source concentration in the feed medium, cells showed comparable macroscopic profiles and therefore reflected comparable cultivations conditions.

Reduction of P. pastoris genome-scale model

The iMT1026 v3.0 model was used to derive a central carbon metabolism model in two reduction steps, generating *PpaPruned* and *PpaCore*. The main characteristics of the reduced model are summarized in Table 2. In order to avoid inconsistencies due to numerical tolerance constraints, 'cof' metabolite corresponding to cofactors in biomass equation was removed. 'COF' reaction has stoichiometric coefficients in the order of 1×10^{-6} that can be lower than the minimal calculation tolerance. By removing COF, no significant impact on the flux distribution or the predictability capacity was observed. In the first reduction step, the 46 reactions were protected. These reactions included the equivalent reactions to the previous *P. pastoris* central carbon metabolism model [24] as well as relevant transport reactions across cell compartments. Protected phenotypes were established in order to ensure the accuracy of the predictions, i.e. the 99.9% of the maximal predicted growth rate in the original model for a given glycerol uptake rate. As reported previously [19], no by-product generation was detected when growing in glycerol-limited chemostats. None of the by-product formation reactions were protected and consequently none were present in *PpaPruned* in agreement with previous experimental data [19]. Initially, the genome scale metabolic model contained 2237 reactions and 1881 metabolites (175 external). As a result of the network reduction, the number of reactions and metabolites was considerably reduced (495 reactions and 513 metabolites). The degrees of freedom (*dof*) were also strongly reduced (from 485 to 4). This could be due to the fact that the pruned model only considers growth on glycerol with no by-product generation. In the subsequent step, *PpaPruned* was further reduced by applying a loss-free network compression step [29], where mainly consecutive, parallel and transport reactions were combined into single reactions. As a result, *PpaCore* was generated including 77 reactions with 102 metabolites with no further reduction in degrees of freedom. The maximal predicted growth rate was identical to that obtained with the original model.

Table 2
Main properties of *P. pastoris* models used and generated in this study.

	iMT1026 v3.0	*PpaPruned*	*PpaCore*	Openflux *PpaCore*
# reactions	2237	495	77	120
# internal metabolites	1706	513	102	100
# external metabolites	175	9	9	9
Maximal biomass generation rate ($g\ gDCW^{-1}\ h^{-1}$)	0.0940	0.0939	0.0939	–

Compared with other models published previously for the same purpose, the present model includes the following characteristics:

- Inclusion of a specific representation of biomass composition and the specific biosynthetic pathways for its precursors.
- Specific oxidative phosphorylation with *P. pastoris* energetic requirements under glycerol growing conditions.
- Glyoxylate pathway
- Complete and specific redox metabolism directly derived from the genome-scale metabolic model.

As the biomass equation is more detailed (includes more compounds), it describes different metabolic situations more accurately, particularly those resulting in a non-growth status when one of its key components cannot be synthesized. The pathways to generate those compounds tend to remain in the reduced model as they are essential reactions. In addition, fluxes of precursors towards biomass generation are more accurately described, since the biomass composition used is specific for growth on glycerol, resulting in improved metabolic flux distributions.

^{13}C-Metabolic flux analysis of glycerol-grown cells

The generated model was implemented in OpenFLUX code for ^{13}C-MFA determination as described above (Table S1). Flux values are presented in Fig. 1 as the 95% confidence interval (CI) in order to provide a more informative description of the results taking into account the uncertainty of estimated fluxes [42]. Although flux values expressed as means of the optimal value ± SEM would provide an overview of changes in the estimated fluxes, this would not indicate the real uncertainty of the measurement due to the asymmetry of the interval. Then, in this study metabolic fluxes are expressed as confidence interval boundaries.

There appears to be only one previous study analysing the metabolic flux distribution of glycerol-grown yeasts based on ^{13}C-labelling experiments [20] using metabolic flux ratio analysis (METAFoR) and thus absolute metabolic flux values were not provided. Moreover, such analysis was limited to the pyruvate node and tricarboxylic acid cycle (TCA) due to the limitations caused by the use of a 3-carbon source such as glycerol. Notably, the flux ratios derived from the metabolic flux calculations performed in the present study are consistent with those obtained using METAFoR analysis. In particular, [20] reported a very low activity through the glyoxylate cycle. This observation was based on the absence of carbon labelling patterns compatible with the activity

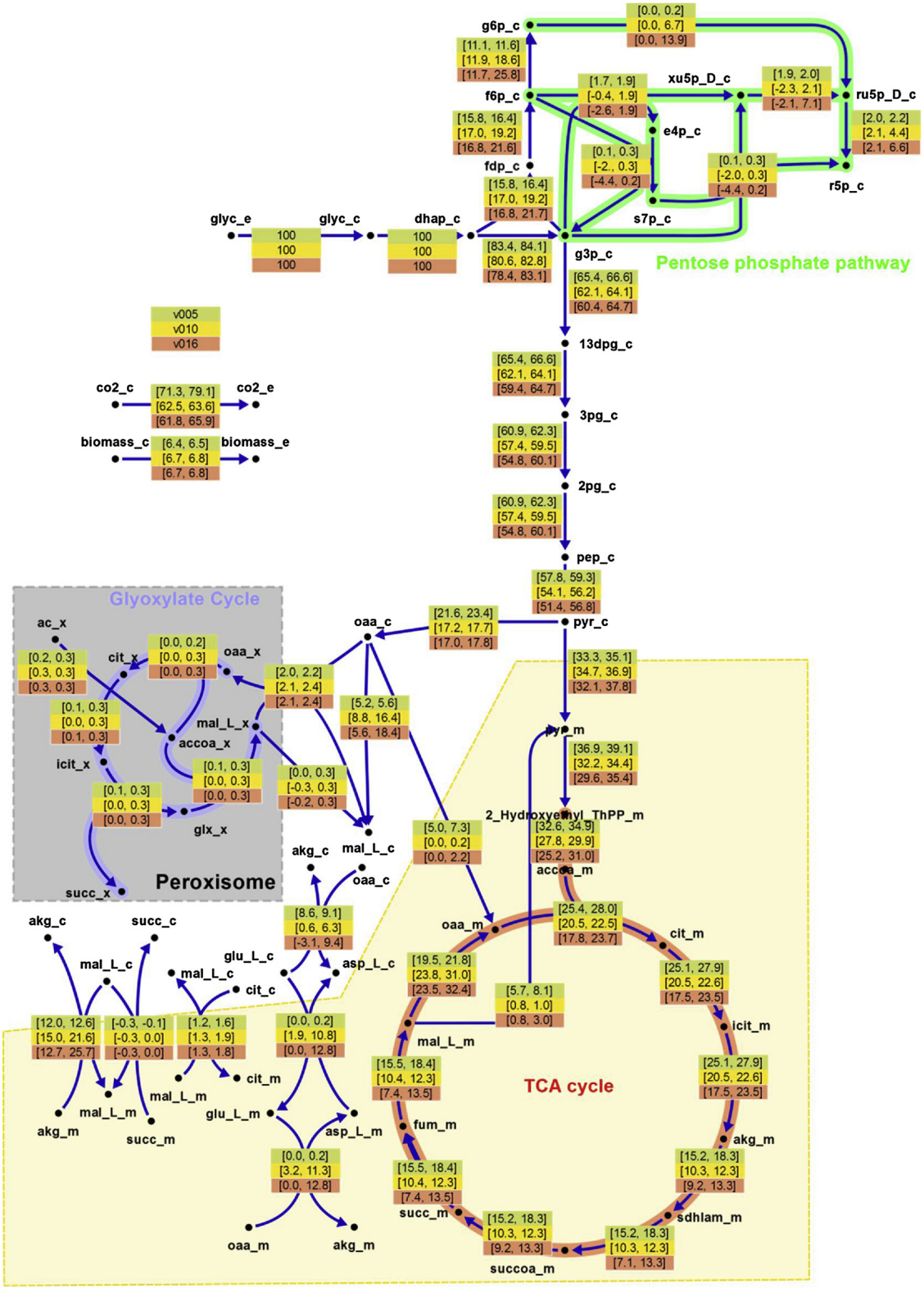

Fig. 1. Metabolic flux distribution estimated for *P. pastoris* growing on glycerol at different dilution rates. 0.05 h^{-1} (top box), 0.10 h^{-1} (middle box) and 0.16 h^{-1} (bottom box). Results are expressed as the 95% confidence interval (CI) of the estimated fluxes relative to the glycerol uptake rate in mmol glycerol · g_{DCW}^{-1} h^{-1}. Lower and upper bounds of CI correspond to the maximum and minimum CI bounds between the replicates. Flux directionality assumption was represented by arrows; therefore, negative fluxes describe opposite direction.

of this pathway, also supported by previous studies in *S. cerevisiae* and *P. stipitis* [47]. In addition, the activity of isocitrate lyase (ICL) was measured [20], showing basal levels in both glucose- and glycerol-grown *P. pastoris* chemostats. Since glucose is known to repress the glyoxylate pathway in *S. cerevisiae* [48] and measured activities of ICL in *P. pastoris* were similar for glucose and glycerol, it was concluded that the flux through glyoxylate cycle was negligible. This consideration has also been subsequently assumed in later studies [24,49–52] by omitting the glyoxylate pathway from the metabolic network for ^{13}C-MFA. As shown in Fig. 1, the activity through glyoxylate cycle found in the present study was very low, almost negligible and thus confirms the previous assumptions in [20]. A second observation by these authors was that the fraction of mitochondrial pyruvate derived from malate was also very low or negligible, thus indicating that the malic enzyme is likewise almost inactive in cells growing on glycerol-limited chemostats. Our calculations are in agreement with this observation. However, for the lowest dilution rate tested (0.05 h^{-1}), the relative flux through the malic enzyme reaction appears to be higher than at the other dilution rates. Nevertheless, this flux is less than 20% of the carbon flux contribution to the mitochondrial pyruvate pool.

The flux split ratio between gluconeogenesis and pentose phosphate pathway cannot be assessed when using biosynthetically directed fractional ^{13}C labelling of proteinogenic amino acids based on uniformly labelled glycerol or glycerol/methanol mixtures [8,20]. Nevertheless, when applying the global fitting approach, fluxes through the oxidative branch of the pentose phosphate pathway (PPP) have been estimated for cells growing under such conditions [9]. Consistent with these previous studies [9], the results described here indicate that the flux through the oxidative branch of PPP was almost negligible (Fig. 1). Thus, most of the NADPH generated in the cytosol would be produced in other reactions, such as glycerol oxidation. Flux directionality in the non-oxidative branch of PPP could only be determined within the 95% CI for cells growing at D = 0.05 h^{-1}. In the other two conditions tested, estimated CI included both reaction directions as feasible (Fig. 1). This uncertainty in estimated PPP fluxes has been previously described and attributed to the operation of PPP reactions close to the thermodynamic equilibrium, i.e. bidirectionally feasible [53].

The resulting core model included several mitochondrial transporters that also act as redox shuttles [54]. Nevertheless, the malate/aspartate shuttle appears to be the major redox shuttle and TCA cycle intermediate metabolite transporter (Fig. 1), while the flux through other transporters was estimated to be very low, almost negligible. High exchange rates of mitochondrial/cytosolic oxaloacetate were observed in previous studies on glycerol [20]. The authors suggested the existence of a highly active mitochondrial shuttle. Moreover, in cultivations on mixtures of glycerol and methanol, a high level of transcription of genes involved in the malate/aspartate shuttle was reported [25]. Thus, those previous studies support the present results that point at the malate/aspartate shuttle as the major redox shuttle and TCA cycle intermediate metabolites transporter.

Impact of dilution rate on metabolic flux distribution

Although the flux through the oxidative branch of PPP was very low, and could therefore be considered as negligible, the upper bound of the CI of the relative flux through the oxidative part of PPP appeared to increase with the growth rate while the uncertainty in the measured data is similar. Hence, while cultivations at 0.05 h^{-1} are estimated to have a relative flux of between 0 and 0.2, those at 0.10 and 0.16 h^{-1} showed a CI upper bound of 6.7 and 13.9 respectively. This would suggest that at higher growth rates, the average relative flux through the oxidative branch of PPP is in fact higher than at lower growth rates. Consequently, the upper bounds for the non-oxidative part of the PPP are also increased at higher growth rates. As recently detailed for *P. pastoris* [19], the growth rate hypothesis (GRH) describes a positive correlation between the growth rate and the RNA and protein content [55–57]. Moreover, the analysis performed of RNA content of cells growing on glycerol at different growth rates also depicts this positive correlation [19]. Considering that major precursors for nucleic acids biosynthesis are generated in the PPP [45], an additional demand for RNA would require an increase in PPP activity. Thus, the estimated increase in relative flux through the oxidative branch of PPP at high growth rates is consistent with the additional demand for RNA precursors, in agreement with the GRH recently described for *P. pastoris* [19]. Concomitantly, the split ratio between gluconeogenesis-PPP and lower glycolysis at the glyceraldehyde 3-phosphate node is also altered with the growth rate. As a result of the increase in the relative flux though gluconeogenesis and PPP at higher growth rates, there is a reduction of relative flux through the lower glycolysis part and consequently to the TCA cycle (Fig. 1). Similar results were reported in [9] in chemostat cultivations using mixtures of glycerol and methanol as carbon sources at low and high dilution rates (0.05 and 0.16 h^{-1}). Among the different mixtures of glycerol and methanol tested, a qualitative comparison of the present results with the reported condition at lower methanol:glycerol ratio (20:80, w/w) can be performed. In this study [9], invariant absolute fluxes through the TCA cycle (citrate synthase reaction) were observed when comparing low and high growth rates, while the substrate uptake rate was much higher at the highest growth rate. Thus, the flux through citrate synthase reaction relative to the substrate uptake rate was significantly reduced at the high growth rate, in agreement with the present results.

A correlation with the relative flux through the malate/α-ketoglutarate transporter and the growth rate was also observed. The upper bound of the CI increases with the dilution rate, thus the relative flux for D = 0.16 h^{-1} would be the highest possible with respect to the other conditions. These results are also in agreement with those described by [20]. The authors reported that at higher growth rates the cytosolic-mitochondrial exchange flux of oxaloacetate was largely unidirectional from the cytosol to the mitochondria. A flux increase in malate/α-ketoglutarate exchange reaction is consistent with the increased unidirectional transport of oxaloacetate into the mitochondria, previously observed under similar growth conditions [20], as malate is subsequently oxidised to oxaloacetate in this organelle. That is, a flux increase in the malate/α-ketoglutarate shuttle could in fact reflect an increase of the oxaloacetate transport net flux into the mitochondria.

Redox cofactor regeneration and energy metabolism

Redox cofactors were excluded from the metabolic flux calculation step using carbon labelling data in order to avoid biased solutions. Consequently, metabolic fluxes were derived exclusively from the adjustment of experimental MIDs to the calculated metabolic isotope distribution and measured input/output fluxes with no interference from other additional information. Once the metabolic fluxes were estimated, a calculation of both oxygen and cofactor regeneration was performed in order to check whether the estimated solution implicitly satisfied the electron balance. Initially, the estimated flux distribution solution predicted an excess of cytosolic NADH that could not be oxidised. Cells have redox shuttles that are able to transport NADH indirectly from cytosol to mitochondria [54]. One such redox shuttle is the malate-aspartate shuttle. In this particular case, despite being present in *PpaCore*, the exact specific activity of the mitochondrial shuttle cannot be calculated as no carbon rearrangement takes place. Consequently, only the net flux in the shuttle system can be calculated (i.e. the difference between the cytosolic and mitochondrial fluxes). Therefore, scaled fluxes in both compartments would result in identical relative flux distributions, but with additional amounts of NADH being translocated to the mitochondria. Regarding the inability to predict scaled up fluxes in redox shuttles employing the currently used constraints, an additional flux fitting was performed by adding the cytosolic NAD(H) balance to the stoichiometric matrix for flux estimation. As a result, identical flux distributions were obtained for reactions other

than the mitochondrial redox shuttle. Moreover, the increase in flux of the mitochondrial redox shuttle in the new calculation corresponds exactly to the calculated excess of cytosolic NADH. Correspondingly, the theoretical oxygen consumption rates were calculated assuming that all the NADH excess was consumed in the ETC. Oxygen requirements included in the biomass equation were also taken into account and constrained in the ETC calculations. Thus, for each growth rate, the theoretically calculated oxygen requirements accounted for over 97% of the experimentally determined oxygen consumption rates. Thus, metabolic fluxes and calculated variables are highly consistent with the experimental data.

Using the metabolic flux distributions and a global electron balance, maximal ATP generation rates were also calculated. Growth associated and non-associated maintenance energies were calculated as described in the Materials and Methods. The y-intersection in the regression of maximal ATP generation rates with the growth rate was 1.22 ± 0.48 mmol ATP g_{DCW}^{-1} h^{-1} and corresponded to the NGAME (See Figure S1 for the graphical representation). Despite the difference, this value is comparable with the 2.51 reported previously [19] for cultivations on glycerol. In addition, GAME was estimated to be 88.8 ± 4.1 mmol ATP g_{DCW}^{-1}, which is higher but comparable to the 70.7 mmol ATP g_{DCW}^{-1} calculated in the previous study, given that only 3 different growth rates are available.

It is worth mentioning that the oxidative branch of PPP is usually considered the major source of cytosolic NADPH [49,58]. Nevertheless, the predicted flux through this pathway in this case was very low, almost negligible, in accordance with previous ^{13}C-MFA estimations on mixtures of glycerol and methanol [9]. In fact, those studies suggested that alternative reactions must supply the required cytosolic NADPH, otherwise an NADPH imbalance was observed. An interesting review [16] shows different glycerol catabolic pathways in yeast, including NAD + and NADP + - dependent glycerol dehydrogenases. In addition, the genome-scale metabolic model derived from its recent annotation already included these reaction and enzyme specificity [19]. Consequently, the present GSMM contains all the relevant reactions producing NADPH in the cytosol. As a result of automatic model reduction, which takes into account the global cofactor balance, *PpaCore* contained the $NADP^+$-dependent glycerol oxidation, although previous core models proposed a NAD^+-dependent glycerol oxidation. Therefore, it seems plausible that the $NADP^+$-dependent oxidation of the glycerol pathway is used in glycerol-grown cells. In this way, it would be the major source for cytosolic NADPH formation. An alternative hypothesis can also be considered. Several redox reactions can use both NADP + or NAD + cofactors. Thus, a global review of cofactor specificity, in the genome-scale metabolic model, may result in changes in cofactor specificity for some reactions. In this case, as noted by [59], the genome-scale flux distribution may be improved and, subsequently, the resulting reduced model may also incorporate those other reactions satisfying redox balance.

Conclusions

The use of ^{13}C-positionally labelled glycerol in the steady state CLEs combined with the analysis of the labelling patterns of proteinogenic amino acids allowed, for the first time, a more reliable estimation of metabolic fluxes through the central carbon pathways of *P. pastoris* cells growing on glycerol as sole C-source within an acceptable confidence range. A new protocol was used to determine the metabolic flux distributions of *P. pastoris* growing in glycerol at different dilution rates. The results allowed verification of the previous hypothesis, calculation of energetic parameters and a proposal for alternative cofactor utilization. Furthermore, we have developed and tested a more robust steady state workflow for ^{13}C-MFA of yeast growing on glycerol as sole carbon source, enabling efficient support for glycerol-based metabolic and bioprocess engineering applications.

Acknowledgements

This work was supported by the projects CTQ2013- 42391-R and CTQ2016-74959-R (AEI/FEDER, UE) of the Spanish Ministry of Economy, Industry and Competitiveness, 2014-SGR-452 of the Reference Network in Biotechnology (XRB) (Generalitat de Catalunya) and the grant FPU FPU12/06185 (M.T.) of the Spanish Ministry of Education, Culture and Sport and the Short-Term Fellowship (M.T.) of the European Molecular Biology Organisation. In addition, the authors would like to acknowledge partial support from the ERA- IB IPCRES project.

Appendix A. Supplementary data

Supplementary material related to this article can be found, in the online version, at doi:https://doi.org/10.1016/j.nbt.2019.01.005.

References

[1] Kiss AA, Grievink J, Rito-Palomares M. A systems engineering perspective on process integration in industrial biotechnology. J Chem Technol Biotechnol 2015;90:349–55. https://doi.org/10.1002/jctb.4584.
[2] Chen Z, Liu D. Toward glycerol biorefinery: metabolic engineering for the production of biofuels and chemicals from glycerol. Biotechnol Biofuels 2016;9:205. https://doi.org/10.1186/s13068-016-0625-8.
[3] Valerio O, Horvath T, Pond C, Misra M, Mohanty A. Improved utilization of crude glycerol from biodiesel industries: synthesis and characterization of sustainable biobased polyesters. Ind Crops Prod 2015;78:141–7. https://doi.org/10.1016/j.indcrop.2015.10.019.
[4] Johnson DT, Taconi KA. The glycerin glut: options for the value-added conversion of crude glycerol resulting from biodiesel production. Environ Prog Sustain Energy 2007;26:338–48. https://doi.org/10.1002/ep.10225.
[5] Yang F, Hanna MA, Sun R. Value-added uses for crude glycerol-a byproduct of biodiesel production. Biotechnol Biofuels 2012;5:1–10. https://doi.org/10.1186/1754-6834-5-13.
[6] da Silva GP, Mack M, Contiero J. Glycerol: a promising and abundant carbon source for industrial microbiology. Biotechnol Adv 2009;27:30–9. https://doi.org/10.1016/j.biotechadv.2008.07.006.
[7] Posada JA, Rincón LE, Cardona CA. Design and analysis of biorefineries based on raw glycerol: addressing the glycerol problem. Bioresour Technol 2012;111:282–93. https://doi.org/10.1016/j.biortech.2012.01.151.
[8] Solà A, Jouhten P, Maaheimo H, Sánchez-Ferrando F, Szyperski T, Ferrer P. Metabolic flux profiling of *Pichia pastoris* grown on glycerol/methanol mixtures in chemostat cultures at low and high dilution rates. Microbiology 2007;153:281–90. https://doi.org/10.1099/mic.0.29263-0.
[9] Jordà J, De Jesus SS, Peltier S, Ferrer P, Albiol J. Metabolic flux analysis of recombinant *Pichia pastoris* growing on different glycerol/methanol mixtures by iterative fitting of NMR-derived 13C-labelling data from proteinogenic amino acids. N Biotechnol 2014;31:120–32. https://doi.org/10.1016/j.nbt.2013.06.007.
[10] Çelik E, Ozbay N, Oktar N, Çalık P. Use of biodiesel byproduct crude glycerol as the carbon source for fermentation processes by recombinant Pichia pastoris. Ind Eng Chem Res 2008;47:2985–90. https://doi.org/10.1021/ie071613o.
[11] Cos O, Ramón R, Montesinos JL, Valero F. Operational strategies, monitoring and control of heterologous protein production in the methylotrophic yeast *Pichia pastoris* under different promoters: a review. Microb Cell Fact 2006;5:17. https://doi.org/10.1186/1475-2859-5-17.
[12] Gasser B, Prielhofer R, Marx H, Maurer M, Nocon J, Steiger M, et al. *Pichia pastoris*: protein production host and model organism for biomedical research. Future Microbiol 2013;8:191–208. https://doi.org/10.2217/fmb.12.133.
[13] Anastácio GS, Santos KO, Suarez PAZ, Torres FAG, De Marco JL, Parachin NS. Utilization of glycerin byproduct derived from soybean oil biodiesel as a carbon source for heterologous protein production in Pichia pastoris. Bioresour Technol 2014;152:505–10. https://doi.org/10.1016/j.biortech.2013.11.042.
[14] Lopes M, Belo I, Mota M. Batch and fed-batch growth of *Pichia pastoris* under increased air pressure. Bioprocess Biosyst Eng 2013;36:1267–75. https://doi.org/10.1007/s00449-012-0871-5.
[15] Ho P-W, Swinnen S, Duitama J, Nevoigt E. The sole introduction of two single-point mutations establishes glycerol utilization in *Saccharomyces cerevisiae* CEN.PK derivatives. Biotechnol Biofuels 2017;10:10. https://doi.org/10.1186/s13068-016-0696-6.
[16] Klein M, Swinnen S, Thevelein JM, Nevoigt E. Glycerol metabolism and transport in yeast and fungi: established knowledge and ambiguities. Environ Microbiol 2017;19:878–93. https://doi.org/10.1111/1462-2920.13617.
[17] Klein M, Carrillo M, Xiberras J, Islam Z, Swinnen S, Nevoigt E. Towards the exploitation of glycerol's high reducing power in *Saccharomyces cerevisiae* -based bioprocesses. Metab Eng 2016;38:464–72. https://doi.org/10.1016/j.ymben.2016.10.008.
[18] Ferrer P, Albiol J. 13C-based metabolic flux analysis in yeast: the *Pichia pastoris* case. Mapelli V, editor. Methods In Molecular Biology, 1152. New York, NY: Springer New York; 2014. p. 209–32. https://doi.org/10.1007/978-1-4939-0563-

8_13.
[19] Tomàs-Gamisans M, Ferrer P, Albiol J. Fine-tuning the *P. Pastoris* iMT1026 genome-scale metabolic model for improved prediction of growth on methanol or glycerol as sole carbon sources. Microb Biotechnol 2018;11:224–37. https://doi.org/10.1111/1751-7915.12871.
[20] Solà A, Maaheimo H, Ylönen K, Ferrer P, Szyperski T. Amino acid biosynthesis and metabolic flux profiling of Pichia pastoris. Eur J Biochem 2004;271:2462–70. https://doi.org/10.1111/j.1432-1033.2004.04176.x.
[21] Maaheimo H, Fiaux J, Petek Çakar Z, Bailey JE, Sauer U, Szyperski T. Central carbon metabolism of *Saccharomyces cerevisiae* explored by biosynthetic fractional 13C labeling of common amino acids. Eur J Biochem 2001;268:2464–79. https://doi.org/10.1046/j.1432-1327.2001.02126.x.
[22] Szyperski T, Glaser RW, Hochuli M, Fiaux J, Sauer U, Bailey JE, et al. Bioreaction network topology and metabolic flux ratio analysis by biosynthetic fractional ^{13}C labeling and two-dimensional NMR spectroscopy. Metab Eng 1999;1:189–97. https://doi.org/10.1006/mben.1999.0116.
[23] Jordà J, Jouhten P, Cámara E, Maaheimo H, Albiol J, Ferrer P. Metabolic flux profiling of recombinant protein secreting *Pichia pastoris* growing on glucose:-methanol mixtures. Microb Cell Fact 2012;11:57. https://doi.org/10.1186/1475-2859-11-57.
[24] Baumann K, Carnicer M, Dragosits M, Graf AB, Stadlmann J, Jouhten P, et al. A multi-level study of recombinant *Pichia pastoris* in different oxygen conditions. BMC Syst Biol 2010;4:141. https://doi.org/10.1186/1752-0509-4-141.
[25] Rußmayer H, Buchetics M, Gruber C, Valli M, Grillitsch K, Modarres G, et al. Systems-level organization of yeast methylotrophic lifestyle. BMC Biol 2015;13:80. https://doi.org/10.1186/s12915-015-0186-5.
[26] Tomàs-Gamisans M, Ferrer P, Albiol J. Integration and validation of the genome-scale metabolic models of *Pichia pastoris*: a comprehensive update of protein glycosylation pathways, lipid and energy metabolism. PLoS One 2016;11:e0148031https://doi.org/10.1371/journal.pone.0148031.
[27] Gopalakrishnan S, Maranas C. Achieving metabolic flux analysis for *S. Cerevisiae* at a genome-scale: challenges, requirements, and considerations. Metabolites 2015;5:521–35. https://doi.org/10.3390/metabo5030521.
[28] Gopalakrishnan S, Maranas CD. 13C metabolic flux analysis at a genome-scale. Metab Eng 2015;32:12–22. https://doi.org/10.1016/j.ymben.2015.08.006.
[29] Erdrich P, Steuer R, Klamt S. An algorithm for the reduction of genome-scale metabolic network models to meaningful core models. BMC Syst Biol 2015;9:48. https://doi.org/10.1186/s12918-015-0191-x.
[30] Hädicke O, Klamt S. *EColiCore2*: a reference network model of the central metabolism of *Escherichia coli* and relationships to its genome-scale parent model. Sci Rep 2017;7:39647. https://doi.org/10.1038/srep39647.
[31] Baumann K, Maurer M, Dragosits M, Cos O, Ferrer P, Mattanovich D. Hypoxic fed-batch cultivation of *Pichia pastoris* increases specific and volumetric productivity of recombinant proteins. Biotechnol Bioeng 2008;100:177–83. https://doi.org/10.1002/bit.21763.
[32] Liu X, Mortensen UH, Workman M. Expression and functional studies of genes involved in transport and metabolism of glycerol in Pachysolen tannophilus. Microb Cell Fact 2013;12:27. https://doi.org/10.1186/1475-2859-12-27.
[33] Knudsen PB, Workman M, Nielsen KF, Thykaer J. Development of scalable high throughput fermentation approaches for physiological characterisation of yeast and filamentous fungi. Kongens Lyngby: Technical University of Denmark; 2015.
[34] Fernandez CA, Des Rosiers C, Previs SF, David F, Brunengraber H. Correction of ^{13}C Mass Isotopomer Distributions for Natural Stable Isotope Abundance. J Mass Spectrom 1996;31:255–62. 10.1002/(SICI)1096-9888(199603)31:3 < 255::AID-JMS290 > 3.0.CO;2-3.
[35] Van Winden WA, Wittmann C, Heinzle E, Heijnen JJ. Correcting mass isotopomer distributions for naturally occurring isotopes. Biotechnol Bioeng 2002;80:477–9. https://doi.org/10.1002/bit.10393.
[36] Quek L-E, Wittmann C, Nielsen LK, Krömer JO. OpenFLUX: efficient modelling software for 13C-based metabolic flux analysis. Microb Cell Fact 2009;8:25. https://doi.org/10.1186/1475-2859-8-25.
[37] Christensen B, Nielsen J. Isotopomer analysis using GC-MS. Metab Eng 1999;1:282–90. https://doi.org/10.1006/mben.1999.0117.
[38] Noorman HJ, Romein B, Luyben KC, Heijnen JJ. Classification, error detection, and reconciliation of process information in complex biochemical systems. Biotechnol Bioeng 2000;49:364–76. 10.1002/(SICI)1097-0290(19960220)49:4 < 364::AID-BIT2 > 3.0.CO;2-N.
[39] Klamt S, Saez-Rodriguez J, Gilles ED. Structural and functional analysis of cellular networks with *CellNetAnalyzer*. BMC Syst Biol 2007;1:2. https://doi.org/10.1186/1752-0509-1-2.
[40] Caspi R, Altman T, Billington R, Dreher K, Foerster H, Fulcher CA, et al. The MetaCyc database of metabolic pathways and enzymes and the BioCyc collection of Pathway/Genome Databases. Nucleic Acids Res 2014;42:459–71. https://doi.org/10.1093/nar/gkt1103.
[41] Antoniewicz MR, Kelleher JK, Stephanopoulos G. Elementary metabolite units (EMU): a novel framework for modeling isotopic distributions. Metab Eng 2007;9:68–86. https://doi.org/10.1016/j.ymben.2006.09.001.
[42] Antoniewicz MR, Kelleher JK, Stephanopoulos G. Determination of confidence intervals of metabolic fluxes estimated from stable isotope measurements. Metab Eng 2006;8:324–37. https://doi.org/10.1016/j.ymben.2006.01.004.
[43] Droste P, Miebach S, Niedenführ S, Wiechert W, Nöh K. Visualizing multi-omics data in metabolic networks with the software Omix—A case study. Biosystems 2011;105:154–61. https://doi.org/10.1016/j.biosystems.2011.04.003.
[44] Pirt SJ. Maintenance energy: a general model for energy-limited and energy-sufficient growth. Arch Microbiol 1982;133:300–2. https://doi.org/10.1007/BF00521294.
[45] Stephanopoulos GN, Aristidou AA, Nielsen J. Review of cellular metabolism. Metab. Eng. San Diego: Academic Press; 1998. p. 21–79. https://doi.org/10.1016/B978-012666260-3/50003-0.
[46] Taccari M, Canonico L, Comitini F, Mannazzu I, Ciani M. Screening of yeasts for growth on crude glycerol and optimization of biomass production. Bioresour Technol 2012;110:488–95. https://doi.org/10.1016/j.biortech.2012.01.109.
[47] Fiaux J, Cakar ZP, Sonderegger M, Wuthrich K, Szyperski T, Sauer U. Metabolic-Flux profiling of the yeasts *Saccharomyces cerevisiae* and *Pichia stipitis*. Eukaryot Cell 2003;2:170–80. https://doi.org/10.1128/EC.2.1.170-180.2003.
[48] Gancedo JM. Yeast carbon catabolite repression. Microbiol Mol Biol Rev 1998;62:334–61.
[49] Jordà J, Rojas H, Carnicer M, Wahl A, Ferrer P, Albiol J. Quantitative metabolomics and instationary 13C-metabolic flux analysis reveals impact of recombinant protein production on trehalose and energy metabolism in Pichia pastoris. Metabolites 2014;4:281–99. https://doi.org/10.3390/metabo4020281.
[50] Nocon J, Steiger MG, Pfeffer M, Sohn SB, Kim TY, Maurer M, et al. Model based engineering of *Pichia pastoris* central metabolism enhances recombinant protein production. Metab Eng 2014;24:129–38. https://doi.org/10.1016/j.ymben.2014.05.011.
[51] Heyland J, Fu J, Blank LM, Schmid A. Quantitative physiology of *Pichia pastoris* during glucose-limited high-cell density fed-batch cultivation for recombinant protein production. Biotechnol Bioeng 2010;107:357–68. https://doi.org/10.1002/bit.22836.
[52] Celik E, Calik P, Oliver SG. Metabolic flux analysis for recombinant protein production by*Pichia pastoris* using dual carbon sources: effects of methanol feeding rate. Biotechnol Bioeng 2010;105:317–29. https://doi.org/10.1002/bit.22543.
[53] Jordà J, Suarez C, Carnicer M, ten Pierick A, Heijnen JJ, van Gulik W, et al. Glucose-methanol co-utilization in *Pichia pastoris* studied by metabolomics and instationary 13C flux analysis. BMC Syst Biol 2013;7:17. https://doi.org/10.1186/1752-0509-7-17.
[54] Bakker BM, Overkamp KM, van Maris AJ, Kötter P, Luttik MAH, van Dijken JP, et al. Stoichiometry and compartmentation of NADH metabolism in Saccharomyces cerevisiae. FEMS Microbiol Rev 2001;25:15–37. https://doi.org/10.1111/j.1574-6976.2001.tb00570.x.
[55] Kyle M, Acharya K, Weider LJ, Looper K, Elser JJ. Coupling of growth rate and body stoichiometry in *Daphnia*: a role for maintenance processes? Freshw Biol 2006;51:2087–95. https://doi.org/10.1111/j.1365-2427.2006.01639.x.
[56] Elser JJ, Acharya K, Kyle M, Cotner J, Makino W, Markow T, et al. Growth rate-stoichiometry couplings in diverse biota. Ecol Lett 2003;6:936–43. https://doi.org/10.1046/j.1461-0248.2003.00518.x.
[57] Franklin O, Hall EK, Kaiser C, Battin TJ, Richter A. Optimization of biomass composition explains microbial growth-stoichiometry relationships. Am Nat 2011;177:E29–42. https://doi.org/10.1086/657684.
[58] Blank LM, Lehmbeck F, Sauer U. Metabolic-flux and network analysis in fourteen hemiascomycetous yeasts. FEMS Yeast Res 2005;5:545–58. https://doi.org/10.1016/j.femsyr.2004.09.008.
[59] Pereira R, Nielsen J, Rocha I. Improving the flux distributions simulated with genome-scale metabolic models of Saccharomyces cerevisiae. Metab Eng Commun 2016;3:153–63. https://doi.org/10.1016/j.meteno.2016.05.002.